HDL-TR-1960
September 1982

Air Target Models for Fuzing Simulations

by John F. Dammann, Jr.

U.S. Army Electronics Research
and Development Command
Harry Diamond Laboratories
Adelphi, MD 20783

UNCLASSIFIED

SECURITY CLASSIFICATION OF THIS PAGE *(When Data Entered)*

REPORT DOCUMENTATION PAGE	READ INSTRUCTIONS BEFORE COMPLETING FORM
1. REPORT NUMBER: HDL-TR-1960	2. GOVT ACCESSION NO.: AD-A121473
3. RECIPIENT'S CATALOG NUMBER:	
4. TITLE *(and Subtitle)*: Air Target Models for Fuzing Simulations	5. TYPE OF REPORT & PERIOD COVERED: Technical Report
	6. PERFORMING ORG. REPORT NUMBER:
7. AUTHOR(s): John F. Dammann, Jr.	8. CONTRACT OR GRANT NUMBER(s):
9. PERFORMING ORGANIZATION NAME AND ADDRESS: Harry Diamond Laboratories, 2800 Powder Mill Road, Adelphi, MD 20783	10. PROGRAM ELEMENT, PROJECT, TASK AREA & WORK UNIT NUMBERS: Program Ele: 6 26.03.A
11. CONTROLLING OFFICE NAME AND ADDRESS: U.S. Army Armament Research and Development Command, Dover, NJ 07801	12. REPORT DATE: September 1982 13. NUMBER OF PAGES: 49
14. MONITORING AGENCY NAME & ADDRESS *(If different from Controlling Office)*:	15. SECURITY CLASS. *(of this report)*: UNCLASSIFIED 15a. DECLASSIFICATION/DOWNGRADING SCHEDULE:

16. DISTRIBUTION STATEMENT *(of this Report)*

Approved for public release; distribution unlimited.

17. DISTRIBUTION STATEMENT *(of the abstract entered in Block 20, if different from Report)*

18. SUPPLEMENTARY NOTES

DRCMS Code: 612603.H.180011
HDL Project: A182J4

19. KEY WORDS *(Continue on reverse side if necessary and identify by block number)*

Radar cross section
Air target encounter simulation
RCS

20. ABSTRACT *(Continue on reverse side if necessary and identify by block number)*

Radar backscatter models for air targets suitable for computer simulation of radar fuze-air target encounters are described. These models determine the characteristics of the energy reflected to the fuze when the target is illuminated by a fuze radar. When the target models are coupled with fuze models, the time when the fuze detects the presence of the target can be determined for any arbitrary terminal encounter geometry. Fuze detection times for

DD FORM 1 JAN 73 1473 EDITION OF 1 NOV 65 IS OBSOLETE

UNCLASSIFIED

SECURITY CLASSIFICATION OF THIS PAGE *(When Data Entered)*

20. ABSTRACT (Cont'd)

representative trajectories can be compared with fuze specifications to measure fuze performance or can be used as a part of a simulation of an entire system to determine system performance.

Following one basic methodology, target models have been written for the Fishbed, Foxbat, and Flogger fighter aircraft; the Hind-D helicopter; and the Backfire, Blinder, and B-1 bombers. All of the models are specular point models where the major return is assumed to come from a small number of glitter points or specular points on the target. The simulations were developed after close scrutiny of experimental target signature data from velocity-scaled tests of many different fuzes and targets. A primary consideration in model development was to keep the mathematics simple enough to allow the user to develop an intuitive understanding of the results and to keep run time short enough to allow unrestricted use of the models.

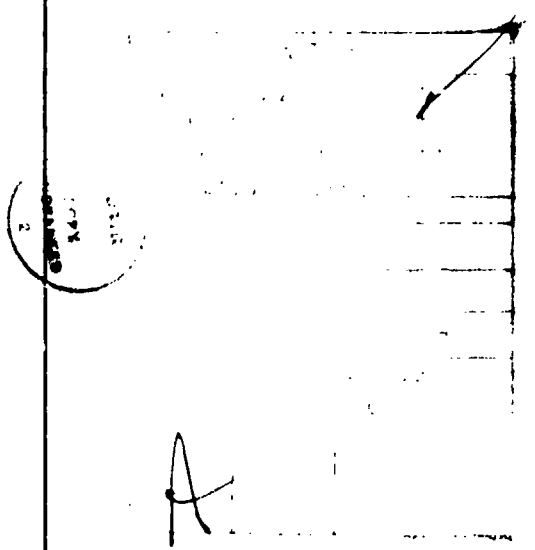

CONTENTS

FIGURES

FIGURES (Cont'd)

TABLES

TABLES (Cont'd)

1. INTRODUCTION

Radar backscatter models for air targets suitable for computer simulation of radar fuze-air target encounters are described in this report. The models are used for analysis of the encounter end game when the missile and the fuze are close to the target. A typical encounter end game is illustrated in figure 1.

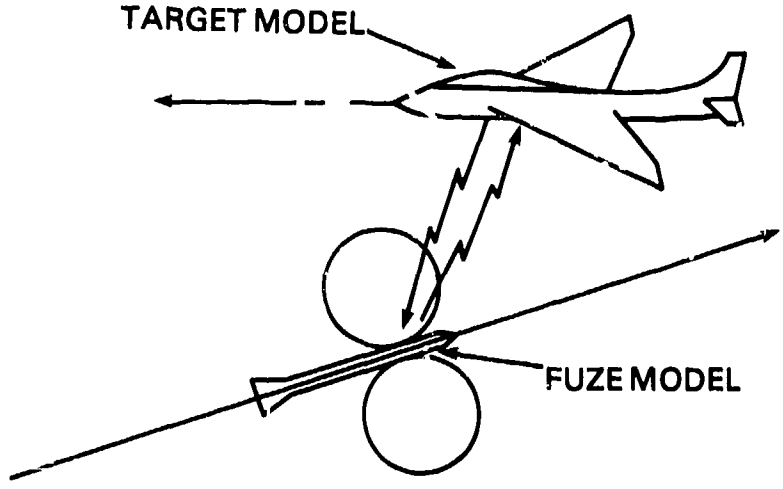

Figure 1. Fuze and target models for end-game fuzing simulation.

The target models determine the characteristics of the energy reflected to the fuze when the target is illuminated by a fuze radar. When the target models are coupled with fuze models, the time when the fuze detects the presence of the target can be computed for any arbitrary terminal encounter geometry. Fuze detection times for representative trajectories can be compared with fuze specifications to measure fuze performance or can be used as part of a simulation of an entire weapon system to determine system performance.

In some cases, fuze performance can be estimated by collecting experimental data from many velocity-scaled, fuze-air target encounters. In many cases, however, there are insufficient resources for running tests to collect target data, or these test data do not fit into existing system simulations. In such cases, the entire determination of fuze performance must be done by computer simulation. Simulation of fuze-air target encounters has already played a key role in measuring fuze performance for major systems such as PATRIOT, ROLAND, and DIVAD and can be expected to play an even larger role in future systems. Thus, development of accurate target models for fuzing is an important step for analysis of fuze performance.

Following one basic methodology, target models have been written for the Fishbed, Foxbat, and Flogger fighter aircraft; the Hind-D helicopter; and the Backfire, Blinder, and B-1 bombers. All of the models are specular point models in which the major return is assumed to come from a small number of glitter points or specular points on the target. The simulations were developed after close scrutiny of experimental target signature data from velocity-scaled tests of many different fuzes and targets.

Previous fuzing models have assumed either a deterministic conical detection beam or a conical beam with some Gaussian variation in the detection beam angle, treated by a Monte Carlo simulation. Target detection was handled by a "first metal" assumption; that is, detection occurred as soon as any part of the target entered the fuze detection beam. These models are satisfactory for narrow-beam fuzes in a benign environment, but fail for wide-beam fuzes where fuzing may occur long after the target enters the beam. They fail also in electronic countermeasures (ECM) environments in which a jammer may mask first metal return, but may not mask much stronger return from a later point in the interior of the target. Thus, the fuze may not function on first metal, but may burn through later in the trajectory. A good target model should adequately predict this benign fuze dud or burn through in an ECM environment.

The present target model is developed in three steps. First, the target is approximated by an ensemble of simple geometric shapes such as ogives, cylinders, flat plates, and ellipsoids. Second, the specular point (the point where the surface is perpendicular to the incident rays) is located on each shape. All the return is assumed to come from these specular points, and the strength of the return from each point is assumed to depend on the local curvatures of the surface at that point. Third, the returns from all specular points are summed vectorially to yield the total target return.

The first step in the development is standard in radar cross section (RCS) analysis and is described by Crispin and Siegel,[1] the Radar Cross Section Handbook,[2] and other texts. However, the second and third steps are not standard and lead to a model that is better suited to fuzing simulations in which the fuze antenna passes very close to the target. The second step results in

a. A natural movement of the specular points along the target surfaces as the fuze passes by,

---

[1] *J. W. Crispin and K. M. Siegel, Methods of Radar Cross Section Analysis, Academic Press, Inc., New York (1968).*

[2] *G. T. Ruck, D. E. Barrick, W. D. Stuart, and C. K. Krichbaum, Radar Cross Section Handbook, Plenum Publishing Corp., New York (1970).*

b. A natural variation in the intensities of the specular points.

These characteristics are crucial to realistic simulations of target return for fuzing. In the third step, by summing the component returns vectorially, return-signal fading can be modelled, and the transient responses of fuzes also can be modelled.

2. TARGET MODELLING CONCEPTS

For fuze modelling, three regions can be considered--a far field, a near field, and a very near field. In the far field, the distance to the target is large in comparison to the target dimensions. A large amount of both theoretical and experimental work has been done for the far-field region, and the RCS for many targets is quite accurately specified. Theoretical expressions for the RCS for many simple objects are given by Crispin and Siegel.[1] These expressions include contributions from the entire object and are strongly dependent on the angle at which the object is seen. Generally, the exact location of the reflection point on the object is ignored since this aspect of the problem is not important in the far field.

In the near field, the distance to the target is on the order of the target dimensions. For an aircraft, this region extends from about 1 to 50 m. In this region, approximations for the RCS are different from those in the far field. The approach taken is to assume that all the significant return comes from a single specular point on each shape. The RCS (σ) of each specular point is given approximately by

$$\sigma = \pi\rho_1\rho_2 \quad ,$$

where ρ_1 and ρ_2 are the principal radii of curvature. The radii of curvature include both the curvature of the target surface at the specular point and the wave-front curvature. In the near field, the wave-front curvature is as significant in determining the RCS as are the target shapes. Hence, the RCS is generally range dependent. Also, the exact position of the specular point on the object is crucial since this position determines the range attenuation for return from that point, the antenna gain and range weighting for the return, and the doppler frequency of the return.

---

[1] *J. W. Crispin and K. M. Siegel, Methods of Radar Cross Section Analysis, Academic Press, Inc., New York (1968).*

In the very near field, still different techniques must be used to approximate the RCS. Here, the curvature of the wave front is generally predominant over the target shape in determining the RCS. The target is close enough to the fuze antenna so that its antenna pattern may not be well defined, complicating the modelling problem. Also, even a minor component of the target may dominate the RCS if the fuze is very close to that component. Modelling in this region is therefore very difficult.

The target model described here is designed primarily for the near field, where most fuzes operate, but is valid in the far field. The model extrapolates the near-field RCS expressions into the very near field. In general, the fuze is in the very near field of a target component for only a short time. Hence, although the model is not as accurate in this region as it is in the near field, it does provide an approximation that should be adequate for fuzing.

To provide RCS estimates over the wide range of distances, the two principal radii of curvature are calculated from the following equation:

$$\frac{1}{\rho_i} = \frac{1}{R} + \frac{1}{r_i} \quad , \quad i = 1, 2,$$

where R is the distance from the fuze to the point and the r_i are the principal radii of curvature of the surface at the point. At very short ranges, the wave-front curvature dominates the expression and

$$\rho_i = R \quad , \quad i = 1, 2,$$

$$\sigma = \pi R^2 \quad .$$

At very long ranges, in the far field, the surface curvature dominates and

$$\rho_i = r_i \quad , \quad i = 1, 2,$$

$$\sigma = \pi r_1 r_2 \quad .$$

This expression agrees with the basic far-field results given by Crispin and Siegel[1] and the Radar Cross Section Handbook.[2]

---

[1] *J. W. Crispin and K. M. Siegel, Methods of Radar Cross Section Analysis, Academic Press, Inc., New York (1968).*

[2] *G. T. Ruck, D. E. Barrick, W. D. Stuart, and C. K. Krichbaum, Radar Cross Section Handbook, Plenum Publishing Corp., New York (1970).*

For some surfaces like the ogive, where the two principal curvatures are very different (say, $r_1 \ll r_2$), there is an intermediate region where the wave-front curvature dominates in one direction and the surface curvature dominates in the other:

$$\sigma \approx \pi r_1 R \quad , \quad r_1 < R < r_2 \quad .$$

The range dependence of the RCS is illustrated for an ogive with r_1 = 1 m and r_2 = 10 m in figure 2.

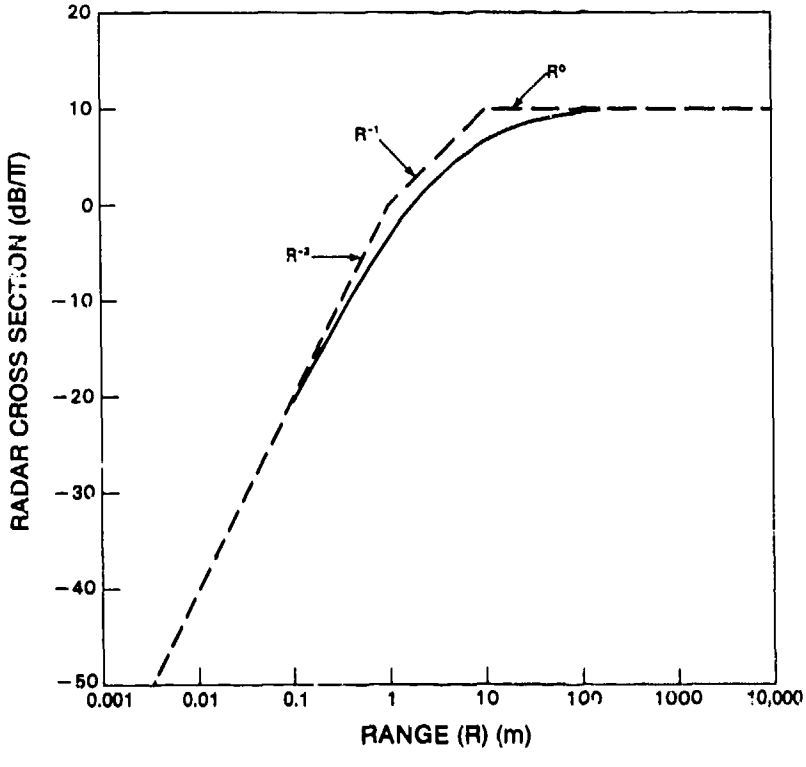

Figure 2. Radar cross section versus range for ogive: r_1 = 1 m and r_2 = 10 m.

Once the RCS of each component has been obtained, the returns must be summed to yield the total target return. In this model, the phase of the return from each point is derived, and the returns are summed vectorially. It is not expected that the model will be precise enough to estimate accurately the instantaneous phases of the returns. Accurate instantaneous phases are not important for fuze applications since in general they change very rapidly in comparison to fuze integration

times. However, the model does approximate the return-signal fading, whose characteristics are of interest in fuze design. Also, it provides an actual doppler voltage waveform for use in simulations of the fuze doppler processors, allowing a much better approximation of these processors than can be assayed with only the average return power available as an input. In particular, the characteristics of the processor transient response can be very accurately modelled.

The model of the MiG-21 is useful in illustrating the modelling techniques. The 10 basic shapes used to approximate this aircraft are combined in figure 3 in a perspective drawing of the aircraft and are listed in table 1. The stationary point reflector at the cockpit is indicated in the figure by an x. For the lower fuze frequencies (ultrahigh frequency--uhf), only the first four of these shapes--the large smooth surfaces where return is truly specular--are significant. For higher fuze frequencies, however, smaller surfaces and corner reflecting surfaces 5 through 10 also become significant. The corner reflecting surfaces do not have true specular points since a double bounce occurs off the surface rather than a single bounce, but they are treated in the model in essentially the same manner as the specular surfaces.

The target model is used in the encounter simulation as shown in figure 4. At each sampling instant, the RCS's and the positions of the specular points are supplied by the model. The position information is used to calculate the range R to each point and the angle θ that the point makes with respect to the fuze antenna. The range attenuation ($1/R^4$), the range gate weighting at R, and the two-way antenna gain at θ are applied to determine the amplitude of return from the point. The rate of change in range with time also determines the doppler frequency of the return. Because the fuze and the target are close, the range attenuation, the range gate weighting, the antenna weighting, and the doppler frequency all may change significantly over the breadth of the target.

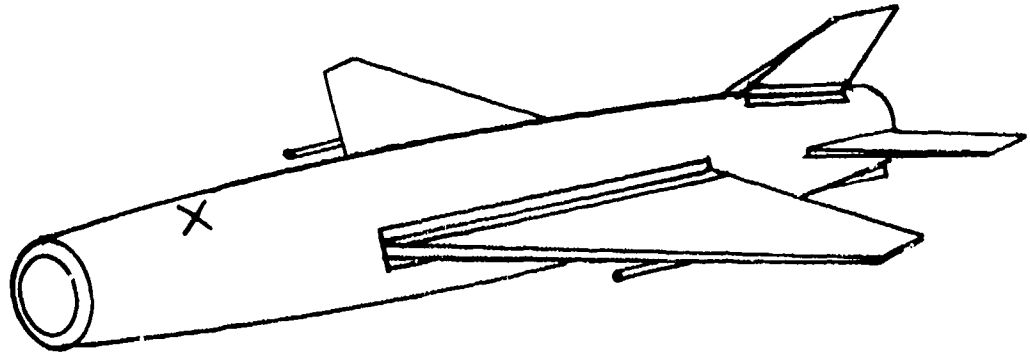

Figure 3. Perspective view of MiG-21 model.

TABLE 1. SPECULAR POINTS FOR MIG-21 MODEL

Point	Scatterer	Surface
1	Fuselage	Ellipsoid
2	Wings	Trapezoidal flat plates
3	Tail fins	Trapezoidal flat plates
4	Vertical stabilizer	Trapezoidal flat plate
5	Wing roots	Dihedral corner reflectors
6	Cockpit	Point reflector
7	Wing store, port	Cylinder
8	Wing store, starboard	Cylinder
9	Vertical stabilizer root	Dihedral corner reflectors
10	Tail drag root	Dihedral corner reflectors

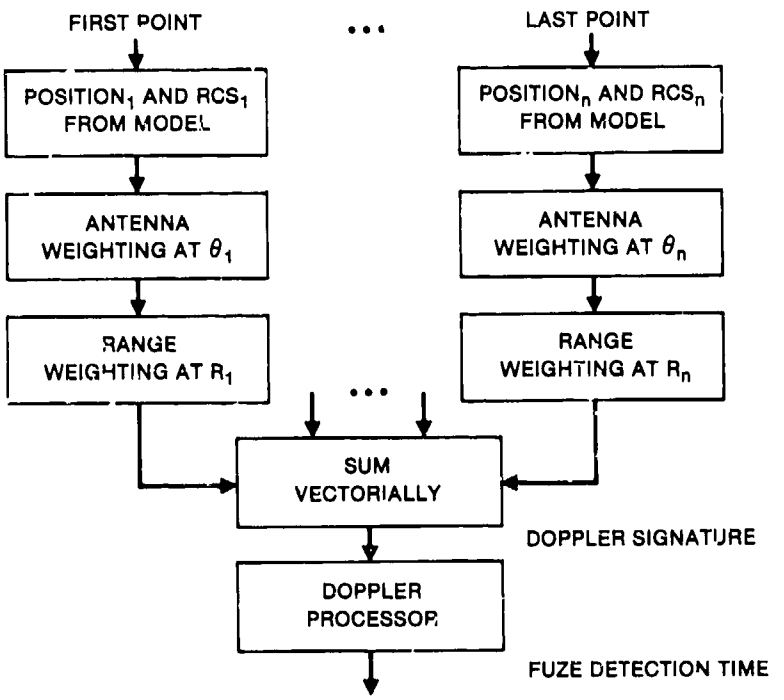

Figure 4. Interaction of fuze and target models in simulation.

The returns from all the points are summed vectorially to yield a voltage-time doppler waveform, or doppler signature, from the target. The phase (ϕ_i) of the return from the ith point is given by

$$\phi_i = 4\pi R_i/\lambda + \xi \quad ,$$

where R_i is the range to the ith point, λ is the wavelength, and ξ is a constant phase that is the same for all points. The first term is due to the two-way path length to the point, and the second is a phase introduced by the fuze receiver and mixers. Thus, the phases of the returns come naturally out of the target model.

3. MODEL DEVELOPMENT

A large volume of data has been collected by the Harry Diamond Laboratories (HDL) for radar fuzes against air targets in velocity-scaled tests. These tests were conducted at an indoor model range at the Encounter Simulation Laboratory (ESL) facility of the Naval Weapons Center and at outdoor ranges at China Lake, CA, and the HDL facility at Blossom Point, MD. In all the tests, the fuze was carried at low velocity past a full-scale target model with the fuze transmitter and the radio frequency (rf) section activated. The return energy was mixed with the transmitted signal to obtain a baseband doppler signal, and the doppler signal was recorded on magnetic tape. In the laboratory, the data were sped up by the appropriate factor to simulate return from a full-speed encounter.

The experimental data were analyzed on a PRIME-400 minicomputer system that includes analog-to-digital (A/D) channels for digitizing experimental data and extensive graphics facilities to aid in interpretation of the data. The target model development has benefited from the very close linkage with the experimental data.

Target backscatter modelling was initiated for wide-beam fuzes, and the model was validated for two of these fuzes. The first validation was done for the MiG-21 target and an experimental uhf fuze with a dipole antenna pattern.[3] The second was done for the MiG-21 target and a developmental fuze operating at a higher frequency with an antenna beam somewhat narrower than the dipole pattern.* For both these fuzes, experimental target signatures were available for many hundreds of

[3] *J. F. Dammann, Air Target-Radar Fuze Encounter Model, The Technical Cooperation Program Technical Panel W6, Sixth Annual Meeting, III, KTA-3 Air Defense (1977).*

**J. F. Dammann, Validation of a Radar Backscatter Model for Aircraft Targets to be used for Fuzing Simulation, Harry Diamond Laboratories, to be published. (CONFIDENTIAL)*

trajectories with a wide range of approach angles and miss distances. Fuzing positions obtained from these experimental data were compared with fuzing positions predicted by the simulation with good agreement.[3,*] For both fuzes, differences between the experimental and simulated fuzing positions were on the order of variations in experimental results due to fuze-to-fuze variations or minor target variations.

Two techniques have been used in the study of the experimental data: (1) spectral analysis of the target doppler signatures using three-dimensional (3-D) plots and (2) analysis of the signatures using a dynamic graphics display. The first technique for data analysis is illustrated in figure 5, a 3-D spectrum plot of doppler return from a sphere using a fuze with a wide-beam antenna. The figure shows a sequence of power spectra, where power is plotted against doppler frequency. The third axis, time or relative position, proceeds from the front to the back of the figure. Each curve is the spectrum of a short segment of signal, and each successive curve is delayed a small amount in time. This method of presenting the spectrum provides a time history of the entire encounter. In the encounter shown, the fuze approaches the sphere at a constant velocity, passing directly beneath the sphere at a 6-m miss distance. The plot shows the doppler frequency of the return decreasing as the fuze approaches, until the frequency is zero when the fuze is directly beneath the sphere. The frequency then increases again as the fuze passes beyond the target. (The small spectral component near 0 Hz is due to experimental noise.)

A 3-D spectrum for a MiG-21 target and a wide-beam fuze is given in figure 6. The aircraft spectra show many tracks like the track from the sphere. The frequency of the return from each specular point and the changes in frequency with time (position) can be estimated closely from the plot. Also evident are three crucial features that a realistic target model must have. First, the significant return comes from a small number of discrete points. Second, since the fuze antenna beam is wide and the tracks often appear and disappear abruptly, the intensity of the points must be dependent on aspect angle. Third, since the slopes of the tracks (changes of frequency with position) are different, some points must move along the aircraft as the fuze passes by.

---

[3] *J. F. Dammann, Air Target-Radar Fuze Encounter Model, The Technical Cooperation Program Technical Panel W6, Sixth Annual Meeting, III, KTA-3 Air Defense (1977).*

**J. F. Dammann, Validation of a Radar Backscatter Model for Aircraft Targets to be used for Fuzing Simulation, Harry Diamond Laboratories, to be published. (CONFIDENTIAL)*

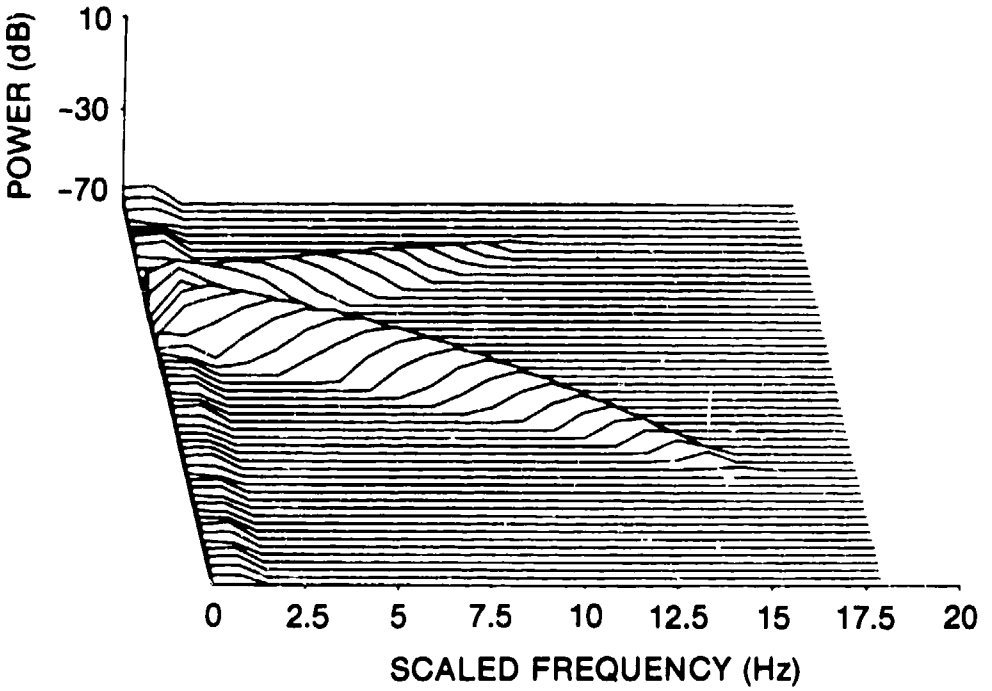

Figure 5. Three-dimensional spectrum for sphere target.

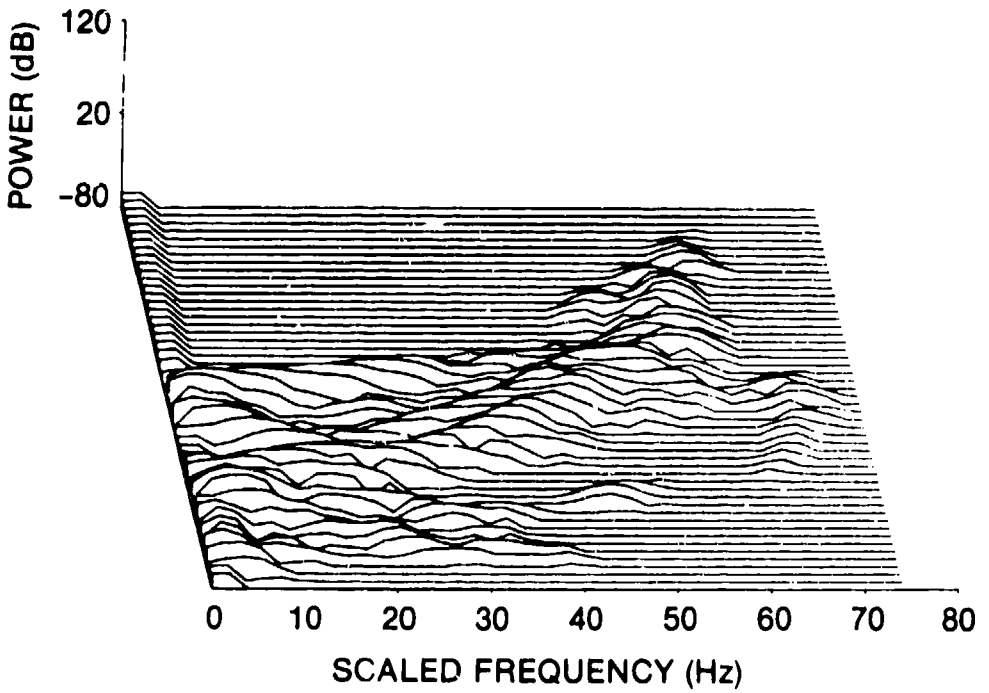

Figure 6. Three-dimensional spectrum for MiG-21 target and wide-beam fuze.

The target modelling recently has been extended to include narrow-beam fuzes. A 3-D spectrum for a U.S. A-4 fighter target and a narrow-beam fuze is shown in figure 7. The tracks of the individual specular points are still evident, although they are now heavily modulated by the antenna pattern so that they appear only in a narrow frequency range. Although the pattern of the tracks here is somewhat easier to discern than usual, the spectrum shown is typical of narrow-beam doppler spectra. The comparison of the wide-beam and narrow-beam spectra indicates that the narrow antenna beam introduces complexities to the modelling, but does not change its basic form. The target modelling job is more complex for narrow-beam fuzes because the major reflectors on the aircraft may not always be within the fuze antenna pattern, and weaker reflectors sometimes dominate the return. Thus, the model needs to be somewhat more detailed. However, the presence of distinct tracks in the narrow-beam spectra indicates that the specular point model is still appropriate.

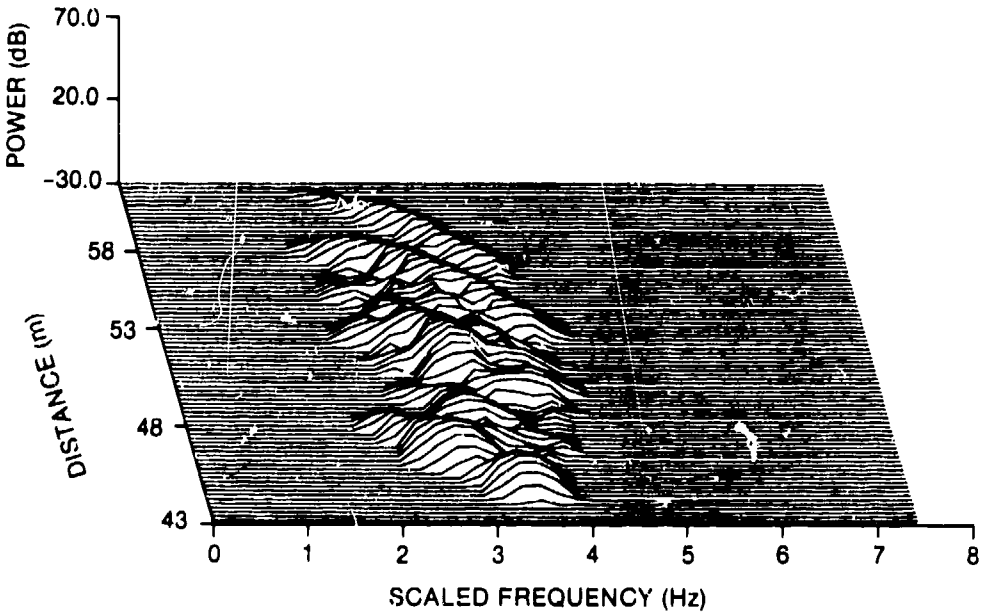

Figure 7. Three-dimensional spectrum for A-4 target and narrow-beam fuze.

Once the basic form of the model had been deduced from the spectra, the model was further developed and refined by using the graphics display program. A sample output of the graphics display program is illustrated in figure 8. In the program, any of three orthogonal views of the target and the missile can be displayed, along with the target

signature and the instantaneous doppler spectrum. The figure shows the top, side, and front views of the aircraft. The target is stationary on the screen, and the missile moves past it along the relative velocity vector (shown as straight lines in the figure).

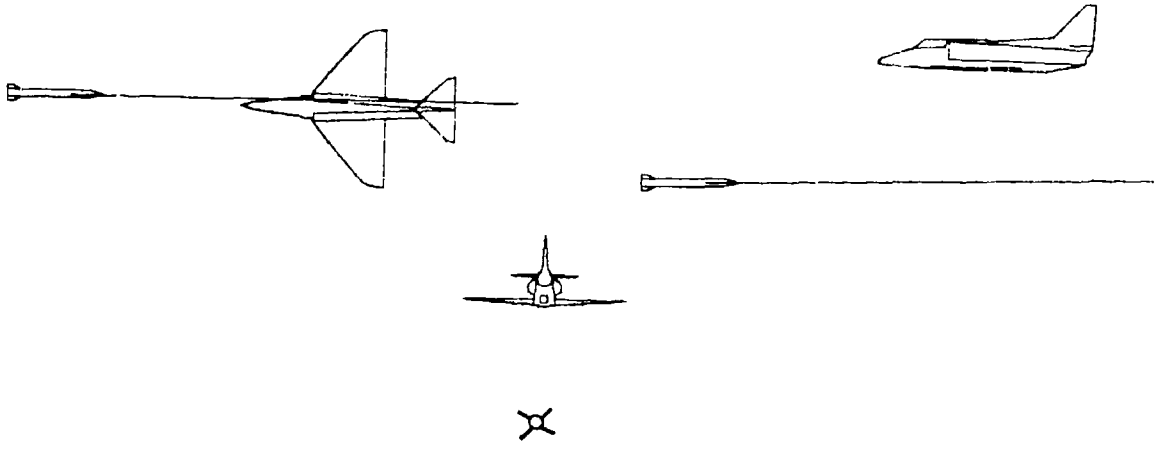

Figure 8. Output from graphics encounter simulation: orthogonal views of A-4 target and missile.

Figure 9 shows the side view of the same encounter with the experimental doppler signature for the encounter. The fuze antenna pattern can be added to any view of the target and is used here to indicate which part of the target is being illuminated at the instant shown. The two radial lines at the edge of the pattern indicate the 10-dB points of the antenna gain pattern, and the two inner radial lines indicate the center of the pattern. The approximate low and high 3-dB points for the fuze range gate also are shown. The star on the signature plot (at about -8 m) marks the voltage at the particular instant shown, enabling the operator to visualize the encounter geometry at that instant and thus to estimate what components of the target contribute to the return.

Figure 10 shows another feature of the graphics encounter simulation. The instantaneous doppler spectrum is shown with the same side view of the encounter. The doppler frequency of return from the specular points in the model can be calculated and compared with the experimental spectrum shown. If the position of the specular point is right, then its doppler frequency will match the experimental, and if the position is wrong, the difference in frequency can be used to adjust the point. Along with the encounter geometry and the doppler signature, the spectrum provides a useful tool for adjusting model parameters.

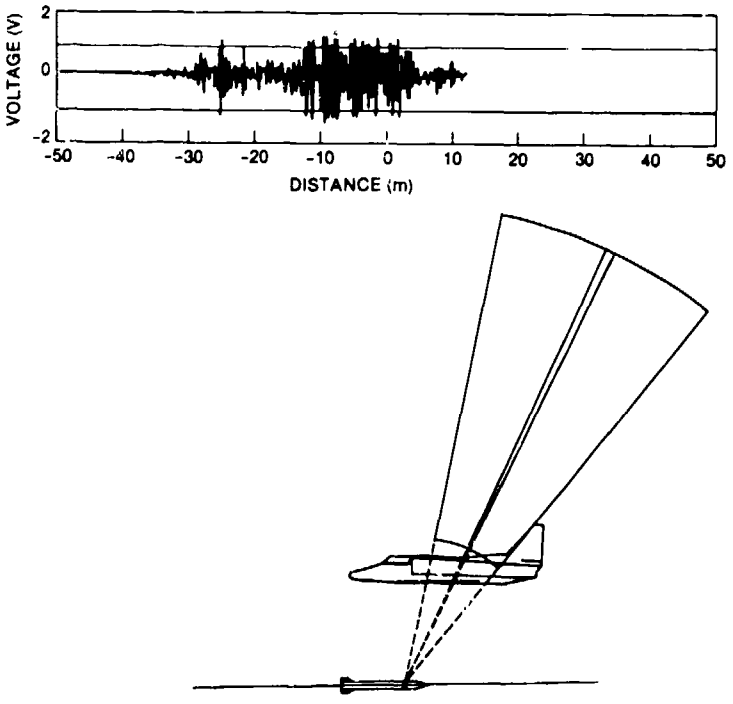

Figure 9. Output from graphics encounter simulation: target and experimental doppler signature.

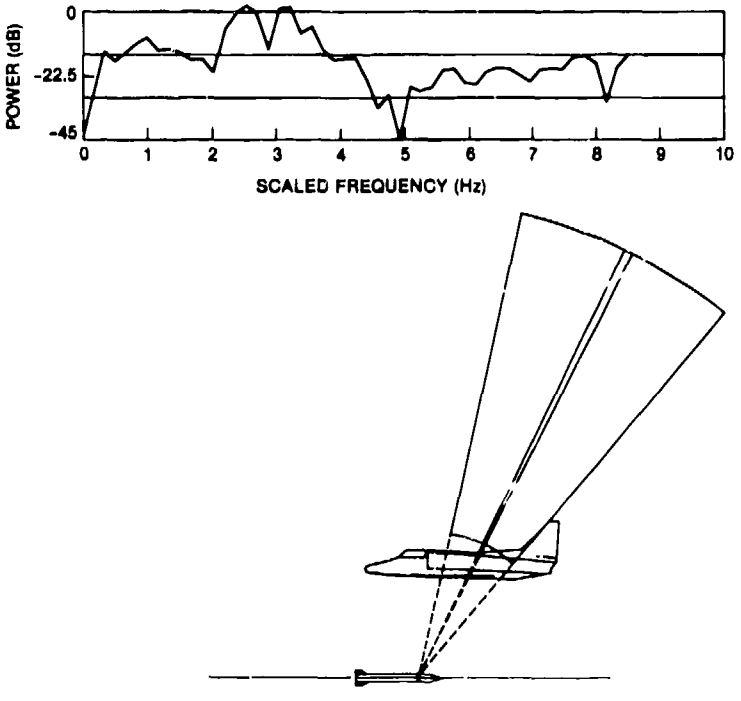

Figure 10. Output from graphics encounter simulation: target and instantaneous doppler spectrum.

4. GENERAL TYPES OF REFLECTORS

This section describes the general types of reflecting surfaces addressed by the target model. The geometric shapes used to approximate the surfaces and the positioning of specular points on these surfaces are discussed, and formulas for the RCS's of the specular points are given. The target models are implemented in the target-based coordinate system shown in figure 11. (In the computer code, this system is referred to as the double prime or pp system.)

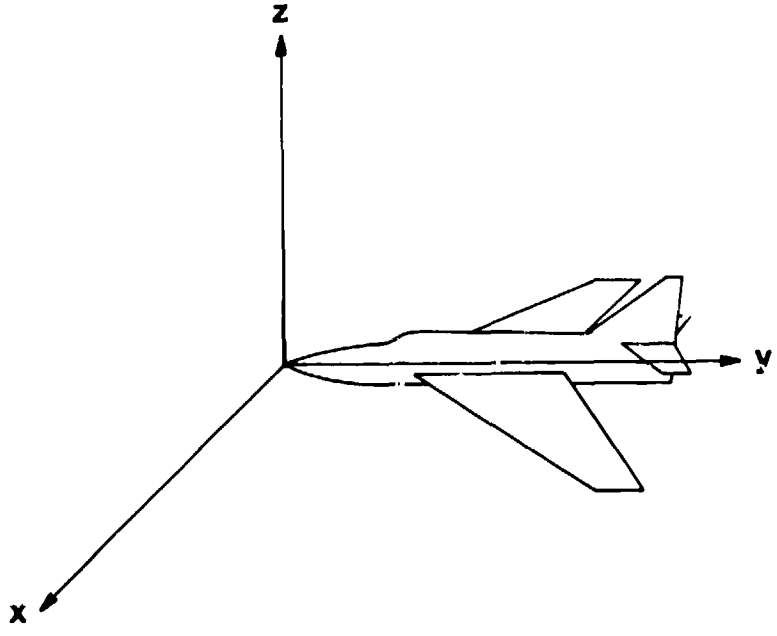

Figure 11. Coordinate system for target modelling.

4.1 Fuselage

The fuselage is the most important reflecting surface of the target since the fuze usually sees this component first. In particular, the curvature of the fuselage is crucial in determining when the fuze first sees a strong reflection and, thus, when fuzing is likely to occur. The geometric shape used to approximate the fuselage is a critical aspect of the model, therefore, and this shape varies from model to model. For example, an ellipsoid is used for the MiG-21, a cylinder and an elongated parallelogram are used for the MiG-25, and an ogive and a conic section are used for the Blinder. Where two or more shapes are used, they are faired into one another to provide a smooth transition in RCS. The particulars of the fuselage modelling for each target are discussed in the sections on individual target models.

4.2 Flat Plate Reflectors

The wings, the tail fins, and the vertical stabilizer are approximated by trapezoidal flat plates. The plates are assumed to have rounded edges so that a true specular point always exists on them. The top and bottom surfaces of these plates are strong reflectors, but the leading and trailing edges of the plates reflect much more weakly. If the specular point is on the root edge of the plate (where it joins the body of the aircraft), then return is assumed to be zero. In this case, there would be no part of the real wing, fin, or stabilizer surface that would be perpendicular to the incident rays. Thus, only one of the wings and one of the tail fins can be visible at any one time, and neither of them is visible when the missile is directly above or below the fuselage.

The computer program first locates the specular point on the surface or the edge of the plate. If the point is on a flat surface, reflection is maximum:

$$\sigma = \pi R^2 \quad ,$$

where R is the distance from the fuze to the specular point. When the point is on the leading or trailing edge of the plate, RCS is a function of the curvature of the edge at the point. This curvature varies depending on the position of the point and on the angle at which the point is viewed. However, in general, the radius of curvature parallel to the wing edge is dominated by the wave-front curvature, while the radius of curvature perpendicular to the wing edge is dominated by the curvature of the wing. This difference suggests the following form for approximating the RCS:

$$\sigma = c\pi aR \quad ,$$

where c is a constant, a is the radius of curvature of the wing edge, and R is the range to the point. Since it is difficult to estimate the wing curvature at all points along its edges, a constant value is assumed. Then the experimental data are used to estimate the product $c \times a$. A reasonable fit to the data is obtained with

$$\sigma = 0.2\pi R \quad .$$

4.3 Dihedral Corner Reflectors

The wing roots, the tail fin roots, the vertical stabilizer root, and the tail drag root are all strong reflectors at higher fuze frequencies. They can all be modelled as dihedral corner reflectors whose dihedral axes are parallel to the y-axis of the model and whose sides are parallel to the x- and z-axes. Define an angle θ in the plane perpendicular to the dihedral axis. The wing root really is two dihedral reflectors--one above the wing and one below, each of which is visible over about 90 deg in θ. In the MiG-21 model, these two reflectors are combined into one reflector that is visible over 180 deg in θ. Over the other 180 deg of θ, the reflector is not visible. Thus, the port wing root is visible only when the fuze is at the port side of the root, and the starboard wing root is visible only when the fuze is at the starboard side of it. In a similar manner, the vertical stabilizer root is visible only at points above the root, and the tail drag is visible only at points below the root.

In general, the RCS of the reflector depends on the angle θ. However, this angle dependence has proven to be complex and difficult to estimate from the experimental data. To keep the model reasonably simple, therefore, the angle dependence has been averaged out.

The RCS depends also on the relative y-coordinates of the fuze and the reflector. If the fuze coordinate is y and the reflector extends from y_1 to y_2, then the experimental data indicate that a reasonable estimate of RCS is

$$\sigma = \begin{cases} 36\left[1 - \dfrac{|y_1 + y_2 - 2y|}{y_2 - y_1}\right], & y_1 < y < y_2 \\ 0, & \text{otherwise.} \end{cases}$$

The specular point is visible only when the fuze y-coordinate is between y_1 and y_2, at which time the point is assumed to be located along the intersection of the two sides of the reflector and to have a y-coordinate equal to that of the fuze.

4.4 Cylindrical Reflectors

Another significant source of backscatter is the aircraft's stores. These stores may have complex shapes, especially when taken with the structures used to attach them to the aircraft. Furthermore,

different configurations of stores may be used for different missions: a single store or a closely nested group of two or three stores may be used. The model puts a reflector where a store or a nest of stores is expected, approximating the long cylindrical shape of most stores, but not the details of the particular store.

The shape used to approximate the store is a long, thin cylinder with rounded ends. The axis of the cylinder is parallel to the y-axis of the model. Thus, the specular point is allowed movement in the y-direction, but essentially no movement in other directions. If a fuze moves past the reflector extending from y_1 to y_2, then the specular point will be at y_1 as long as the fuze coordinate y is less than y_1. When y equals y_1, the point follows the fuze along the cylinder until y equals y_2. At that time, the specular point remains at y_2 as the missile moves past.

The experimental data indicate that the stores reflect at essentially all angles, except when shadowed by another part of the aircraft. No strong dependence of RCS on incidence angle was observed. Therefore, the RCS of the point is set at a constant value--estimated to be about 4 m^2--where the point is not shadowed.

4.5 Point Reflectors

The final major sources of backscatter approximated by the model are point reflectors such as the cockpit and the air intakes. Typically, these reflectors are complex assemblies with correspondingly complex reflection patterns. Modelling these components precisely is beyond the scope of this model. The RCS of the reflector is therefore assumed to be constant where the point is visible and zero where it is shadowed by the other components of the aircraft. The RCS constant for the point and the region over which it is visible depend on the particular reflector being modelled and are covered in the sections on individual target models.

4.6 Minor Reflectors

In addition to the large specular reflectors described above, there are a large number of weak reflectors on the aircraft. Inspection of any aircraft reveals a number of small irregularities in the aircraft skin--such as antennas, air scoops, and air deflectors--that reflect radar waves. When a major specular reflector is in the antenna beam, it swamps out the return from these minor reflectors. But the return from minor reflectors is sufficient to function a sensitive fuze, and for a

narrow-beam fuze there are situations in which there are no major reflectors in the beam. These situations are especially likely for small miss distances where the antenna illuminates a relatively small portion of the aircraft. Experimental data for small misses indicate that minor reflectors are indeed seen and that they provide sufficient return to function many fuzes.

It is impossible to model these minor reflectors precisely since intelligence data are inadequate to identify all the possible sources and since different versions of an aircraft configured for different missions would be expected to have significantly different sources. Therefore, the model uses point reflectors randomly scattered along the aircraft. Two hundred of the points are placed along the fuselage and 200 are placed along the wings, with each point having a constant RCS. The resulting doppler return approximately matches the experimental data in average power level, although it obviously cannot match the details of the true target signature.

5. MIG-21 MODEL

The particular version of the MiG-21 or Fishbed chosen for modelling is the Fishbed C/E. This version was chosen primarily because full-scale and fifth-scale physical models are available at the ESL test facility, and HDL has collected extensive target signature data from these targets for other fuze programs. The C/E version is distinguished by a somewhat shorter and more ellipsoidal fuselage than later versions.

Aside from differences in dimensions, the MiG-21 target model is distinguished from the other target models primarily by the shape used to approximate the fuselage. An ellipsoidal shape is used (actually, a prolate spheroid since two of its dimensions are the same) with the nose and the tail chopped off. This shape is an excellent approximation to the true fuselage shape.

Three orthogonal views of the shapes used to approximate the MiG-21 are shown in figure 12. The major reflectors on the aircraft are listed in table 2 with their positions and dimensions. Table 3 lists the types of reflectors used to model each of the significant reflecting surfaces. The maximum RCS's for the reflectors also are given, as well as the areas in space from which the reflectors are visible. These two columns summarize the RCS information given in the descriptions of the different types of reflectors in section 4.

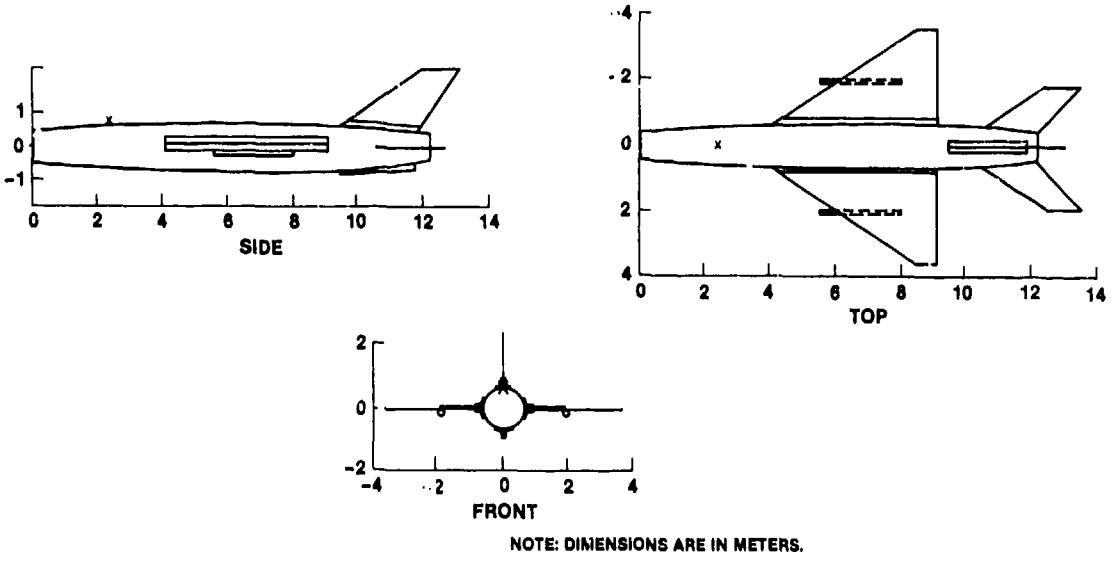

Figure 12. Orthogonal views of MiG-21 model.

TABLE 2. MIG-21 MODEL SHAPES

Point	Scatterer	Point lies on surface (m)
1	Fuselage	Ellipsoid: semiaxes are 0.66, 7.07, and 0.66; center at (0.0,6.1,0.0); ends chopped at y = 0.0 and 12.2
2	Wings	Trapezoidal flat plates with corners at (±0.61,4.0,-0.05), (±0.61,9.1,-0.05), (±3.63,8.47,-0.05), (±3.63,9.1,-0.05)
3	Tail fins	Trapezoidal flat plates with corners at (±0.61,10.55,0.09), (±0.61,12.5,0.09), (±1.9,12.5,0.09), (±1.9,13.53,0.09)
4	Vertical stabilizer	Trapezoidal flat plate with corners at (0.0,9.45,0.61), (0.0,11.9,0.61), (0.0,11.9,2.38), (0.0,13.11,2.38)
5	Wing roots	Lines from (±0.61,4.0,-0.05) to (±0.61,9.1,-0.05)
6	Cockpit	Point at (0.0,2.44,0.91)
7	Wing store, port	Line from (2.0,5.6,-0.05) to (2.0,8.0,-0.05)
8	Wing store, starboard	Line from (-2.0,5.6,-0.05) to (-2.0,8.0,-0.05)
9	Vertical stabilizer root	Line from (0.0,9.45,0.61) to (0.0,11.9,0.61)
10	Tail drag root	Line from (0.0,9.45,-0.61) to (0.0,11.9,-0.61)

TABLE 3. MIG-21 MODEL RADAR CROSS SECTIONS

Point	Scatterer	Shape	Max radar cross section	Visibility
1	Fuselage	Ellipsoid	πRr	Everywhere
2	Wings	Trapezoidal flat plate	πR^2	$\|x\| > 0.61$
3	Tail fins	Trapezoidal flat plate	πR^2	$\|x\| > 0.61$
4	Vertical stabilizer	Trapezoidal flat plate	πR^2	$z > 0.51$
5	Wing roots	Dihedral corner reflector	36 m^2	$\|x\| > 0.61$, $4 < y < 9.1$
6	Cockpit	Point reflector	9 m^2	$z > 0.91$
7	Wing store, port	Cylindrical reflector	4 m^2	$5.6 < y < 8$, $z < 0$
8	Wing store, starboard	Cylindrical reflector	4 m^2	$5.6 < y < 8$, $z < 0$
9	Vertical stabilizer root	Dihedral corner reflector	36 m^2	$9.45 < y < 11.9$, $z > 0.61$
10	Tail drag reflector	Dihedral corner reflector	36 m^2	$9.45 < y < 11.9$, $z < -0.61$

Notes:
(x,y,z) are fuze coordinates in target coordinate system.
Aim point is (0,6.1,0).
R is distance from fuze to specular point.
r is radius of fuselage at specular point.

6. MIG-25 MODEL

Version A of the MiG-25 or Foxbat is modelled, the basic interceptor version with a large air-intercept (AI) radar in the nose. Version B, used for reconnaissance, is similar except for a much smaller radar in the nose and a slightly altered wing configuration. For fuze modelling, the radome covering the nose radar is assumed to be transparent so that there is no backscatter from this radome and the AI radar beneath it is visible to the fuze. The AI radar is modelled as a point reflector. The fuselage behind the radome is modelled as a composite of two shapes--a cylinder for the forward section up to the air intakes and an elongated parallelepiped for the rear section.

The shapes used to model the MiG-25 are shown in figure 13. The significant reflectors with their dimensions and RCS's are given in tables 4 and 5.

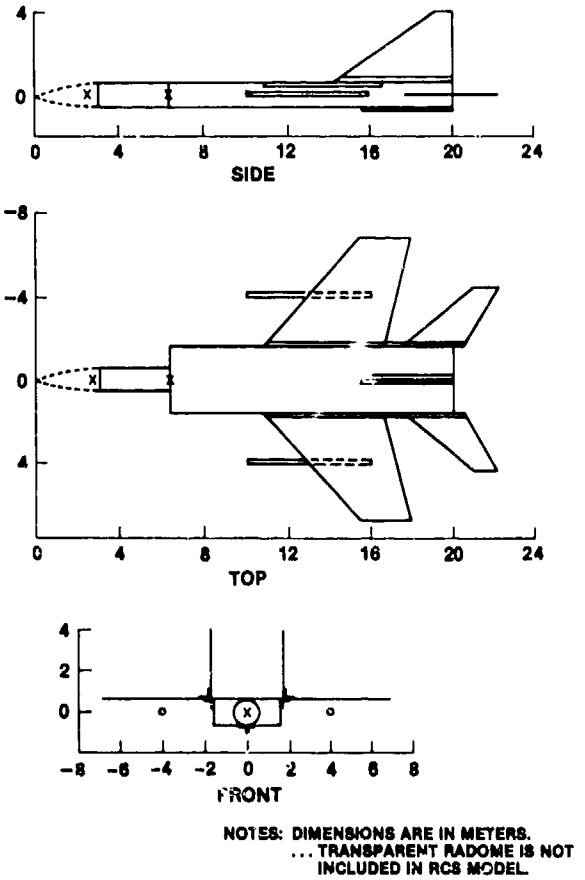

Figure 13. Orthogonal views of MiG-25 model.

TABLE 4. MIG-25 MODEL SHAPES

Point	Scatterer	Point lies on surface (m)
1	Fuselage	Cylinder: y = 3.0 to 6.3, radius = 0.61; elongated parallelepiped: y = 6.3 to 19.9, x = ±1.6, z = ±0.61
2	Wings	Trapezoidal flat plates with corners at (±1.6,10.8,0.61), (±1.6,16.6,0.61), (±6.9,15.6,0.61), (±6.9,17.6,0.61)
3	Tail fins	Trapezoidal flat plates with corners at (±1.6,17.6,0.0), (±1.6,20.6,0.0), (±4.4,21.0,1.6), (±4.4,22.1,0.0)
4	Vertical stablizer, port	Trapezoidal flat plate with corners at (1.7,19.5,4.1), (1.7,20.2,4.1), (1.7,14.4,0.61), (1.7,19.7,0.61)
5	Vertical stabilizer, starboard	Trapezoidal flat plate with corners at (-1.7,19.5,4.1), (-1.7,20.2,4.1), (-1.7,14.4,0.61), (-1.7,19.7,0.61)
6	Wing roots	Line from (±1.6,10.8,0.61) to (±1.6,16.6,0.61)
7	Wing store, port	Line from (4.0,10.0,0.0) to (4.0,15.9,0.0)
8	Wing store, starboard	Line from (-4.0,10.0,0.0) to (-4.0,15.9,0.0)
9	Vertical stabilizer root, port	Line from (1.7,14.4,0.61) to (1.7,19.7,0.61)
10	Vertical stabilizer root, starboard	Line from (-1.7,14.4,0.61) to (-1.7,19.7,0.61)
11	Tail drag root	Line from (0.0,15.7,-0.61) to (0.0,19.2,-0.61)
12	Air scoops and cockpit	Point at (0.0,6.3,0.0)
13	Air-intercept antenna	Point at (0.0,2.5,0.0)

TABLE 5. MIG-25 MODEL RADAR CROSS SECTIONS

Point	Scatterer	Shape	Max radar cross section	Visibility
1	Fuselage	Cylinder and parallelepiped	πRr	$y > 3$
2	Wings	Trapezoidal flat plate	πR^2	$\|x\| > 1.6$
3	Tail fins	Trapezoidal flat plate	πR^2	$\|x\| > 1.6$
4	Vertical stabilizer, port	Trapezoidal flat plate	πR^2	$z > 0.61$
5	Vertical stabilizer, starboard	Trapezoidal flat plate	πR^2	$z > 0.61$
6	Wing roots	Dihedral corner reflector	36 m^2	$\|x\| > 1.6$, $z < 0.61$, $10.8 < y < 16.6$
7	Wing store, port	Cylindrical reflector	4 m^2	$z < 0.61$
8	Wing store, starboard	Cylindrical reflector	4 m^2	$z < 0.61$
9	Vertical stabilizer root, port	Dihedral corner reflector	36 m^2	$14.4 < y < 19.7$, $z > 0.61$
10	Vertical stabilizer root, starboard	Dihedral corner reflector	36 m^2	$14.4 < y < 19.7$, $z > 0.61$
11	Tail drag root	Dihedral corner reflector	36 m^2	$15.7 < y < 19.2$, $z < -0.61$
12	Air scoops and cockpit	Point reflector	4 m^2	Everywhere
13	Air-intercept antenna	Point reflector	4 m^2	Everywhere

Notes:
(x,y,z) are fuze coordinates in target coordinate system.
Aim point is (0,10,0).
R is distance from fuze to specular point.
r is radius of fuselage at specular point (assumed to be 0.61 along cylinder and parallelogram).

7. MIG-27 MODEL

The MiG-27 or Flogger-D is a swept-wing design capable of lower speed and lower altitude flight with its wings swept forward or higher speed and higher altitude flight with its wings swept back. For modelling, the full swept-back position of the wings is assumed since it appears that this configuration is most likely to be encountered by the fuze.

The fuselage is modelled by using a composite of three shapes--an ogive for the nose, a cylinder for the forward section between the nose and the air intakes, and an elongated parallelepiped for the rear section. The three shapes used to approximate the fuselage, as well as the other significant reflectors of the MiG-27, are shown in figure 14. Tables 6 and 7 list the reflectors and their dimensions and RCS's.

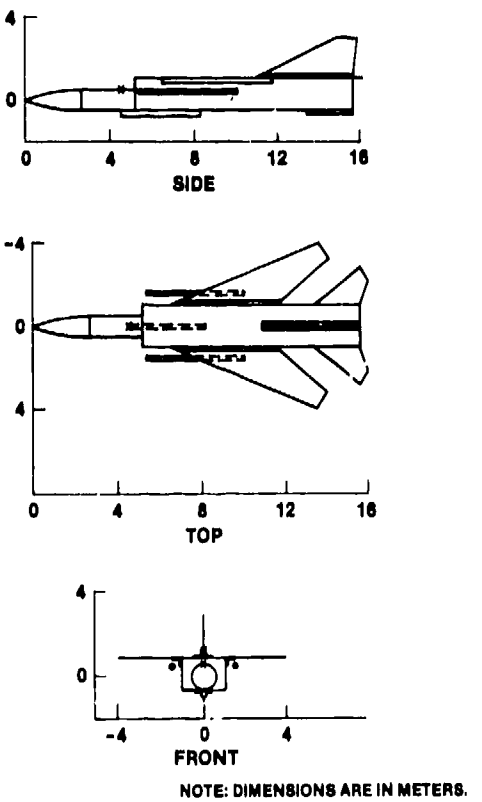

Figure 14. Orthogonal views of MiG-27 model.

TABLE 6. MIG-27 MODEL SHAPES

Point	Scatterer	Point lies on surface (m)
1	Fuselage	Ogive: y = 0.0 to 2.5, max radius = 0.5; cylinder: y = 2.5 to 5.2, radius = 0.5; elongated parallelepiped: y = 5.2 to 15.7, x = ±1.0, z = 1.0,-0.5
2	Wings	Trapezoidal flat plates with corners at (±1.0,11.5,1.0), (±1.0,6.5,1.0), (±3.2,14.1,1.0), (±4.05,13.5,1.0)
3	Tail fins	Trapezoidal flat plates with corners at (±1.0,15.7,0.5), (±1.0,13.4,0.5), (±2.2,16.0,0.5), (±2.75,15.7,0.5)
4	Vertical stabilizer	Trapezoidal flat plate with corners at (0.0,15.7,3.0), (0.0,14.8,3.0), (0.0,15.7,1.0), (0.0,10.8,1.0)
5	Small stores on fuselage	Line from (0.0,4.6,-0.6) to (0.0,8.2,-0.6)
6	Wing roots	Lines from (±1.0,6.5,1.0) to (±1.0,11.5,1.0)
7	Wing store, port	Line from (1.5,5.4,0.4) to (1.5,10.0,0.4)
8	Wing store, starboard	Line from (-1.5,5.4,0.4) to (-1.5,10.0,0.4)
9	Vertical stabilizer root	Line from (0.0,10.8,1.0) to (0.0,15.7,1.0)
10	Air scoops and cockpit	Point at (0.0,4.5,0.5)
11	Tail drag root	Line from (0.0,13.4,-0.5) to (0.0,15.7,-0.5)

TABLE 7. MIG-27 MODEL RADAR CROSS SECTIONS

Point	Scatterer	Shape	Max radar cross section	Visibility
1	Fuselage	Ogive, cylinder, parallelepiped	πRr	Everywhere
2	Wings	Trapezoidal flat plate	πR^2	$\|x\| > 1$
3	Tail fins	Trapezoidal flat plate	πR^2	$\|x\| > 1$
4	Vertical stabilizer	Trapezoidal flat plate	πR^2	$z > 1$
5	Small stores on fuselage	Cylindrical reflector	4 m^2	$z < 0$
6	Wing roots	Dihedral corner reflector	36 m^2	$\|x\| > 1$, $z < 1.0$, $6.5 < y < 11.5$
7	Wing store, port	Cylindrical reflector	4 m^2	$z < 0.4$
8	Wing store, starboard	Cylindrical reflector	4 m^2	$z < 0.4$
9	Vertical stabilizer root	Dihedral corner reflector	36 m^2	$10.8 < y < 15.7$, $z > 1$
10	Air scoops and cockpit	Point reflector	4 m^2	Everywhere
11	Tail drag root	Dihedral corner reflector	36 m^2	$13.4 < y < 15.7$, $z < -0.5$

Notes:
(x,y,z) are fuze coordinates in target coordinate system.
Aim point is (0,7.85,0).
R is distance from fuze to specular point.
r is radius of fuselage at specular point (assumed to be 0.5 for cylinder and parallelepiped).

8. BACKFIRE MODEL

The version of the Backfire chosen for modelling is model B, which is the developed version with landing gear fairings nearly eliminated. The aircraft is a swept-wing design capable of lower speed and lower altitude flight with its wings swept forward or higher speed and higher altitude flight with its wings swept back. For modelling, the full swept-back position of the wings is assumed since it appears that this configuration is most likely to be encountered by the fuze.

The fuselage is the most complex feature of this target to model. It is modelled as a composite of three shapes--an ogive for the nose, a cylinder for the forward section between the nose and the air intakes, and an elongated parallelepiped for the rear section. The three shapes used to approximate the fuselage, as well as the other significant reflectors of the Backfire, are shown in figure 15. Tables 8 and 9 list the reflectors and their dimensions and RCS's.

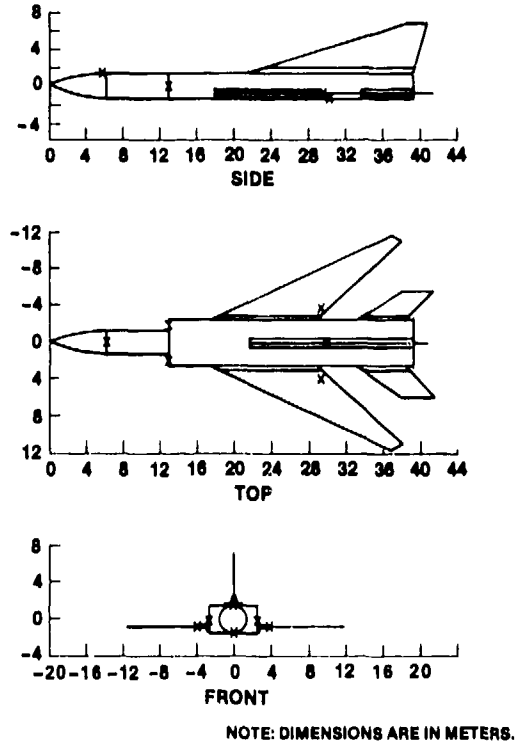

Figure 15. Orthogonal views of Backfire model.

TABLE 8. BACKFIRE MODEL SHAPES

Point	Scatterer	Point lies on surface (m)
1	Fuselage	Ogive: y = 0.0 to 6.0, max radius = 1.45; cylinder: y = 6.0 to 13.0, radius = 1.45; elongated parallelepiped: y = 13.0 to 39.3, x = ±2.5, z = ±1.45
2	Wings	Trapezoidal flat plates with corners at (±2.5,29.0,-0.8), (±2.5,18.0,-0.8), (±11.0,38.0,-0.8), (±11.7,37.0,-0.8)
3	Tail fins	Trapezoidal flat plates with corners at (±2.5,38.8,-0.8), (±2.5,33.0,-0.8), (±5.7,41.6,-0.8), (±5.7,38.0,-0.8)
4	Vertical stabilizer	Trapezoidal flat plate with corners at (0.0,40.5,7.4), (0.0,38.5,7.4), (0.0,39.3,1.45), (0.0,21.0,1.45)
5	Wing roots	Lines from (±2.5,29.0,-0.8) to (±2.5,18.0,-0.8)
6	Vertical stabilizer root	Line from (0.0,39.3,1.45) to (0.0,21.0,1.45)
7	Tail fin roots	Lines from (±2.5,38.8,-0.8) to (±2.5,33.0,-0.8)
8	Cockpit	Point at (0.0,5.8,1.45)
9	Air intake, starboard	Point at (-2.0,13.0,0.0)
10	Air intake, port	Point at (2.0,13.0,0.0)
11	Wheel well, starboard	Point at (-4.0,29.0,-0.8)
12	Wheel well, port	Point at (4.0,29.0,-0.8)
13	Front wheel well	Point at (0.0,11.0,-1.45)
14	Lower protrusion	Point at (0.0,30.0,-1.45)

TABLE 9. BACKFIRE MODEL RADAR CROSS SECTIONS

Point	Scatterer	Shape	Max radar cross section	Visibility
1	Fuselage	Ogive, cylinder, parallelepiped	πRr	Everywhere
2	Wings	Trapezoidal flat plate	πR^2	$\|x\| > 2.5$
3	Tail fins	Trapezoidal flat plate	πR^2	$\|x\| > 2.5$
4	Vertical stabilizer	Trapezoidal flat plate	πR^2	$z > 1.45$
5	Wing roots	Dihedral corner reflector	36 m^2	$\|x\| > 2.5$, $18 < y < 29$
6	Vertical stabilizer root	Dihedral corner reflector	36 m^2	$21 < y < 39.3$, $z > 1.45$
7	Tail fin root	Dihedral corner reflector	36 m^2	$33 < y < 38.8$, $\|x\| > 2.5$
8	Cockpit	Point reflector	4 m^2	$y < 6$, $z > 0$
9	Air intake, starboard	Point reflector	4 m^2	$x < 0$, $y < 13$
10	Air intake, port	Point reflector	4 m^2	$x > 0$, $y < 13$
11	Wheel well, starboard	Point reflector	1 m^2	$z < -0.8$
12	Wheel well, port	Point reflector	1 m^2	$z < -0.8$
13	Front wheel well	Point reflector	1 m^2	$z < -0.8$
14	Lower protrusion	Point reflector	1 m^2	$z < -0.8$

Notes:
(x,y,z) are fuze coordinates in target coordinate system.
Aim point is (0,19.65,0).
R is distance from fuze to specular point.
r is radius of fuselage at specular point (assumed to be 1.45 for cylinder and parallelepiped).

9. BLINDER MODEL

The version of the Blinder chosen for modelling is version A. From a fuze modelling standpoint, version B would be essentially identical and versions C and D also would be very similar. The ESL facility has a fifth-scale physical model of version A, and the mathematical model was constructed to match the ESL dimensions as closely as possible. Mathematical model signatures have been compared with the experimental signatures from the ESL model.*

Three orthogonal views of the shapes used to approximate the Blinder are shown in figure 16. The major reflectors on the aircraft are listed in table 10 with their positions and dimensions. Table 11 lists the types of reflectors used to model each of the significant reflecting surfaces. The maximum RCS's for the reflectors also are given, as well as the areas in space from which the reflectors are visible. These two columns summarize the RCS information given in the descriptions of the different types of reflectors in section 8.

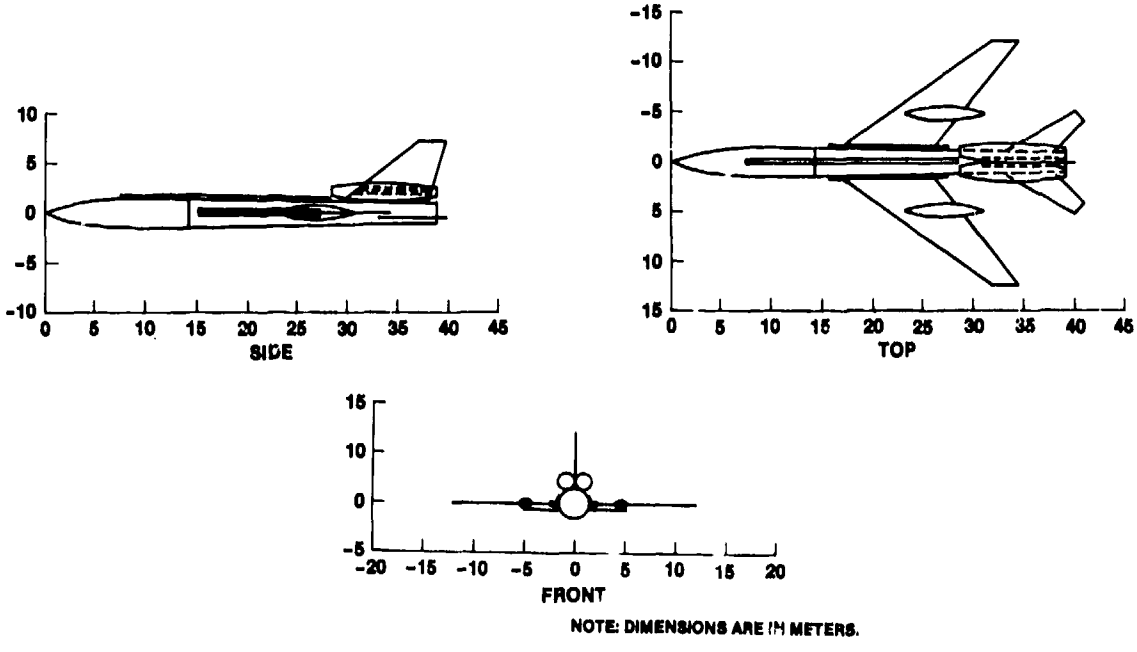

Figure 16. Orthogonal views of Blinder model.

J. F. Dammann, Validation of a Radar Backscatter Model for Aircraft Targets to be used for Fuzing Simulation, Harry Diamond Laboratories, to be published. (CONFIDENTIAL)

TABLE 10. BLINDER MODEL SHAPES

Point	Scatterer	Point lies on surface (m)
1	Fuselage	Ogive: y = 0.0 to 14.0, max radius = 1.5; conic section: y = 14.0 to 38.8, radius = 1.5 at y = 14.0 and 1.0 at y = 38.8
2	Wings	Trapezoidal flat plates with corners at (±1.4,16.8,0.0) (±12.2,31.8,0.0), (±12.2,34.5,0.0), (±1.4,25.9,0.0)
3	Tail fins	Trapezoidal flat plates with corners at (±1.0,33.1,-0.5), (±5.1,40.0,-0.5), (±4.2,40.8,-0.5), (±0.5,37.8,-0.5)
4	Vertical stabilizer	Trapezoidal flat plate with corners at (0.0,29.7,1.7), (0.0,37.7,7.1), (0.0,39.8,7.1), (0.0,38.0,2.2)
5	Wing roots	Lines from (±1.4,15.4,0.0) to (±1.4,27.5,0.0)
6	Engine roots	Line from (0.0,30.6,2.2) to (0.0,38.4,2.2)
7	Engines	Prolate spheroid with center at (±0.9,33.7,2.2), length = 10.4, max radius = 0.9
8	Wing pod, port	Ogive: center at (4.8,27.2,0.0), half length = 4.0, max radius = 0.6
9	Wing pod, starboard	Ogive: center at (-4.8,27.2,0.0), half length = 4.0, max radius = 0.6
10	Cockpit and top ridge	Line from (0.0,7.4,1.2) to (0.0,28.5,1.2)

TABLE 11. BLINDER MODEL RADAR CROSS SECTIONS

Point	Scatterer	Shape	Max radar cross section	Visibility
1	Fuselage	Ogive and cone	πRr	Everywhere
2	Wings	Trapezoidal flat plate	πR^2	$\|x\| > 1.4$
3	Tail fins	Trapezoidal flat plate	πR^2	$\|x\| > 0.5$
4	Vertical stabilizer	Trapezoidal flat plate	πR^2	$z > 1.7$ or $y > 38$
5	Wing roots	Dihedral corner reflector	36 m^2	$\|x\| > 1.4$, $15.4 < y < 27.5$
6	Engine roots	Dihedral corner reflector	9 m^2	$30.6 < y < 38.4$
7	Engines	Prolate spheroid	1 m^2	Everywhere
8	Wing pod, port	Ogive	Min (25.6,1.9R) m^2	Everywhere
9	Wing pod, starboard	Ogive	Min (25.6,1.9R) m^2	Everywhere
10	Cockpit and top ridge	Cylindrical reflector	1 m^2	$z > 1.2$, $y < 28.5$

Notes:
(x,y,z) are fuze coordinates in target coordinate system.
Aim point is (0,25.39,0).
R is distance from fuze to specular point.
r is radius of fuselage at specular point (1.5 m max).

10. B-1 MODEL

The B-1 is an advanced, low-level penetration bomber with a variable geometry wing structure. For fuze modelling, the wings are assumed to be fully swept back. The complex aerodynamic shape of the plane, especially the blended wing and body configuration, makes the target particularly difficult to approximate with simple geometric shapes.

Three orthogonal views of the shapes used to approximate the B-1 are shown in figure 17. The major reflectors on the aircraft are listed in table 12 with their positions and dimensions. Table 13 lists the

types of reflectors used to model each of the significant reflecting surfaces. The maximum RCS's for the reflectors also are given, as well as the areas in space from which the reflectors are visible. These two columns summarize the RCS information given in the descriptions of the different types of reflectors in section 4.

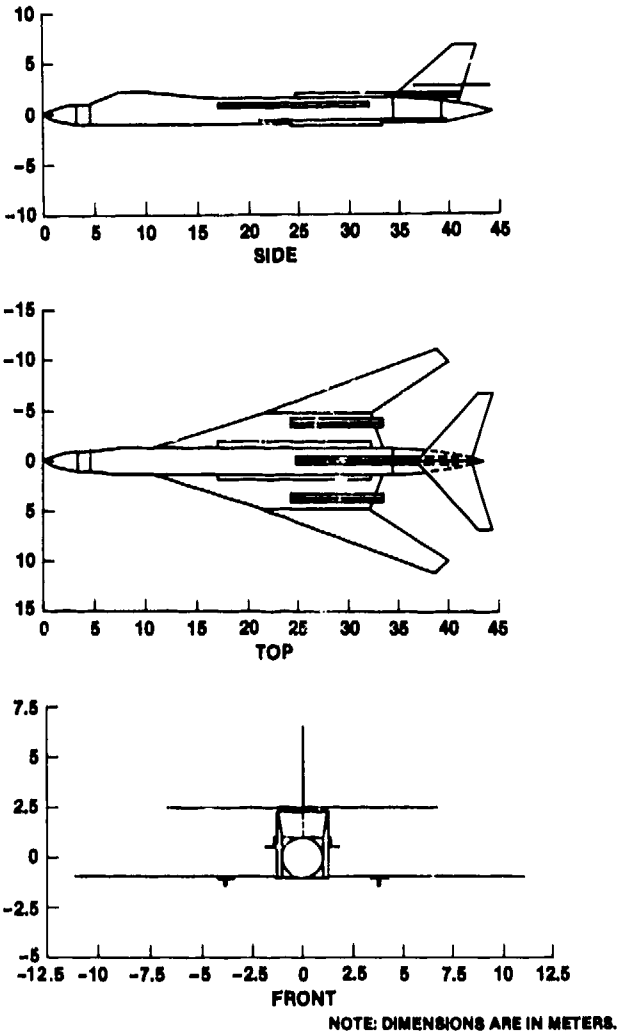

Figure 17. Orthogonal views of B-1 model.

TABLE 12. B-1 MODEL SHAPES

Point	Scatterer	Point lies on surface (m)
1	Fuselage nose	Ogive: y = 0.0 to 3.5, max radius = 1.0; fairing: y = 3.5 to 4.6
2	Fuselage center	Flat plates: y = 4.6 to 16.6
3	Fuselage tail	Flat plates: y = 16.6 to 34.7; fairing: y = 34.7 to 39.0; ogive: y = 39.0 to 44.7, max radius = 1.0
4	Wings	Trapezoidal flat plates with corners at (±4.8,21.4,-0.9), (±11.2,38.7,-0.9), (±10.0,40.0,-0.9), (±4.8,32.2,-0.9)
5	Tail fins	Trapezoidal flat plates with corners at (±0.0,36.7,2.5), (±6.8,43.0,2.5), (±6.8,44.4,2.5), (±0.0,42.1,2.5)
6	Vertical stabilizer	Trapezoidal flat plate with corners at (0.0,34.7,1.4), (0.0,40.7,6.6), (0.0,42.9,6.6), (0.0,41.2,1.0)
7	Wing roots	Lines from (±1.3,16.9,0.5) to (±1.3,32.1,0.5)
8	Engine, port	Line from (3.8,24.3,-0.9) to (3.8,33.4,-0.9)
9	Engine, starboard	Line from (-3.8,24.3,-0.9) to (-3.8,33.4,-0.9)
10	Vertical stabilizer root	Line from (0.0,24.8,1.5) to (0.0,41.2,1.5)
11	Wing fairings	Trapezoidal flat plates with corners at (±1.3,10.5,-1.0), (±4.8,21.4,-1.0), (±4.8,32.2,-1.0), (±1.3,33.2,-1.0)

TABLE 13. B-1 MODEL RADAR CROSS SECTIONS

Point	Scatterer	Shape	Max radar cross section	Visibility
1	Fuselage nose	Ogive and fairing	πRr	$y < 4.6$
2	Fuselage center	Flat plates	πRr	Everywhere
3	Fuselage tail	Flat plates, fairing, and ogive	πRr	$y > 16.6$
4	Wings	Trapezoidal flat plate	πR^2	$\|x\| > 4.8$
5	Tail fins	Trapezoidal flat plate	πRr	Everywhere
6	Vertical stabilizer	Trapezoidal flat plate	πRr	$z > 1.4$ or $y > 41.2$
7	Wing roots	Dihedral corner reflector	36 m^2	$\|x\| > 1.3$, $16.9 < y < 32.1$, $z > 0.5$
8	Engine, port	Dihedral corner reflector	36 m^2	$24.3 < y < 33.4$, $z < -0.9$
9	Engine, starboard	Dihedral corner reflector	36 m^2	$24.3 < y < 33.4$, $z < -0.9$
10	Vertical stabilizer root	Dihedral corner reflector	36 m^2	$24.8 < y < 41.2$, $z > 1.5$
11	Wing fairings	Trapezoidal flat plates	πR^2	$\|x\| > 1.3$

Notes:
(x,y,z) are fuze coordinates in target coordinate system.
Aim point is (0,22.35,0).
R is distance from fuze to specular point.
r is radius of fuselage at specular point (1 m max).

11. HIND-D MODEL

The shapes used to approximate the Hind-D target are shown in figure 18. Tables 14 and 15 list the reflectors and their dimensions and RCS's. The most important feature of the Hind-D model is the moving rotor blades, and the model for these blades is described in detail in this section.

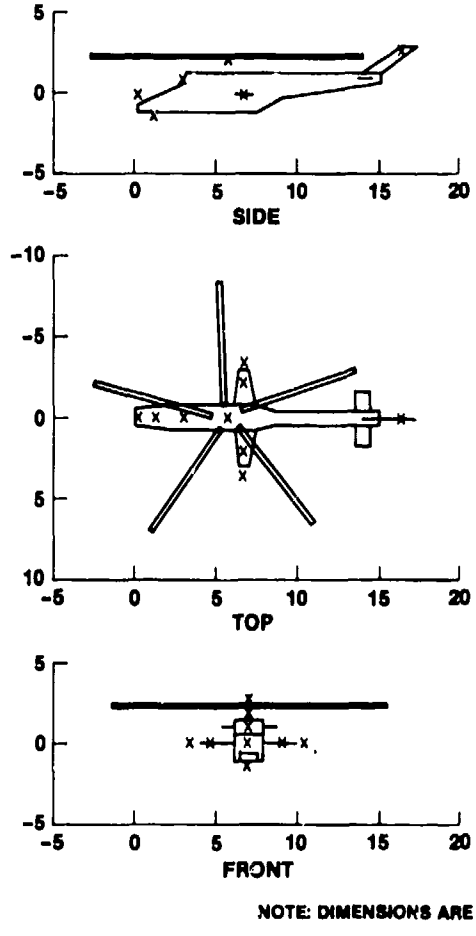

Figure 18. Orthogonal views of Hind-D model.

TABLE 14. HIND-D MODEL SHAPES

Point	Scatterer	Point lies on surface (m)
1	Fuselage	Flat plates: y = 0.0 to 14.9; top, bottom, and sides are functions of y
2	Launch rails	Trapezoidal flat plates with corners at (±0.8,6.2,0.0), (±0.8,7.4,0.0), (±3.0,6.4,0.0), (±3.0,6.9,0.0)
3	Tail fins	Trapezoidal flat plates with corners at (±0.4,13.7,1.0), (±0.4,14.5,1.0), (±1.7,13.7,1.0), (±1.7,14.4,1.0)
4	Vertical stabilizer	Trapezoidal flat plate with corners at (0.0,13.9,1.3), (0.0,14.9,1.3), (0.0,16.3,2.8), (0.0,17.2,2.8)
5	Rotor blades	Ellipsoid and wedge, center at (0.0,5.6,2.4)
.	.	.
.	.	.
.	.	.
9	Rotor blades	Ellipsoid and wedge, center at (0.0,5.6,2.4)
10	Pods below nose	Point at (0.0,1.2,-1.3)
11	Pods above nose	Point at (0.0,0.2,0.0)
12	Lower air scoops	Point at (0.0,3.0,0.9)
13	Rotor hub	Point at (0.0,5.6,2.0)
14	Rockets, inner port rail	Point at (2.2,6.6,0.0)
15	Rockets, inner starboard rail	Point at (-2.2,6.6,0.0)
16	Missiles, outer port rail	Point at (3.5,6.6,0.0)
17	Missiles, outer starboard rail	Point at (-3.5,6.6,0.0)
18	Tail rotor	Point at (0.0,16.3,2.6)

TABLE 15. HIND-D MODEL RADAR CROSS SECTIONS

Point	Scatterer	Shape	Max radar cross section	Visibility
1	Fuselage	Flat plates	πRr	Everywhere
2	Launch rails	Trapezoidal flat plate	πR^2	$\|x\| > 0.8$
3	Tail fins	Trapezoidal flat plate	πR^2	$\|x\| > 0.4$
4	Vertical stabilizer	Trapezoidal flat plate	πR^2	$z > 1.3$
5	Rotor blades	Ellipsoid and wedge	2 m^2	Everywhere
.	.	.	.	.
.	.	.	.	.
.	.	.	.	.
9	Rotor blades	Ellipsoid and wedge	2 m^2	Everywhere
10	Pods below nose	Point reflector	0.1 m^2	$z > 0$
11	Pods above nose	Point reflector	0.1 m^2	$z > 0$
12	Lower air scoops	Point reflector	0.1 m^2	$y < 3$, $z > 0.9$
13	Rotor hub	Point reflector	0.1 m^2	$z > 0$
14	Rockets, inner port rail	Point reflector	0.1 m^2	$z < 0$
15	Rockets, inner starboard rail	Point reflector	0.1 m^2	$z < 0$
16	Missiles, outer port rail	Point reflector	0.1 m^2	$x > 0$
17	Missiles, outer starboard rail	Point reflector	0.1 m^2	$x < 0$
18	Tail rotor	Point reflector	0.1 m^2	Everywhere

Notes:
(x,y,z) are fuze coordinates in target coordinate system.
Aim point is (0,5.60,0).
R is distance from fuze to specular point.
r is radius of fuselage at specular point.

The main rotor blades are important vulnerable components of the Hind-D helicopter. The blade width and depth dimensions are relatively small, and small fragmenting shells must detonate close to a blade in order to damage it. Thus, the precise position where the fuze causes detonation for trajectories passing close to the rotor blades is important in end-game simulation of shells against the Hind-D. For this reason, a rotor blade model was developed that is considerably more detailed and complex than modelling for the rest of the helicopter. The present model is suitable for uhf fuzes only. However, modifications necessary to fit the model to higher frequency fuzes are straightforward.

The Hind-D has five identical blades spaced evenly at 72-deg intervals around the circle. Figure 19 shows one of these blades and the coordinate system used for the blade modelling. This coordinate system is centered at the rotor hub, with the negative y-axis along one of the five blades. An angle θ defines the instantaneous blade rotation such that $\theta = 0$ for the blade pointing straightforward and rotation is in the direction of positive θ (clockwise from above).

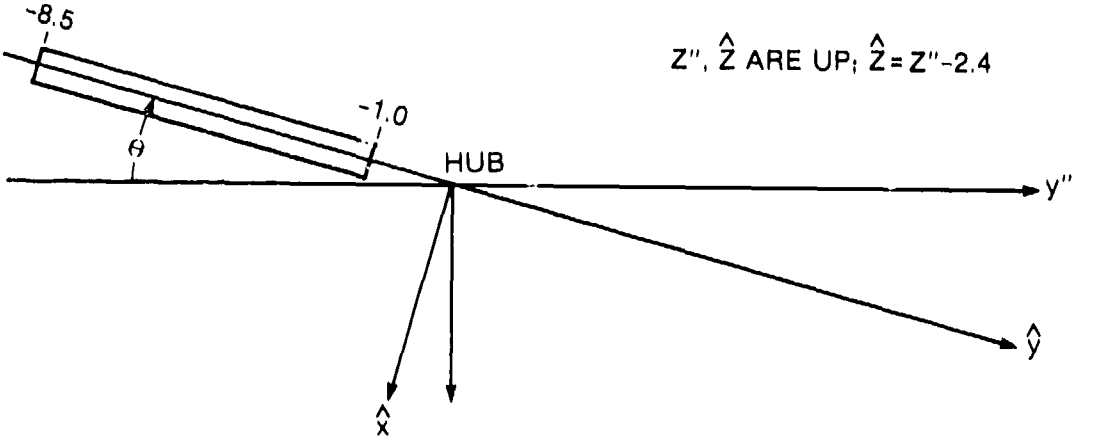

Figure 19. Hind-D rotor blade coordinate system, top view.

The double primed target-based coordinate system used in target modelling is shown for the Hind-D in figure 19. The rotor hub is 5.6 m behind and 2.4 m above the origin of the double primed system, and for zero blade rotation the respective axes of the two coordinate systems are parallel.

Precise dimensions of the blade are taken from drawings of the fifth-scale model used at ESL and verified (approximately) with intelligence information. The blade extends from -1 to -8.5 m along the $\hat{y}$-axis and is assumed to have a constant physical cross section along its entire length. The spar connecting the blade to the hub and the slight contouring of the blade at the ends are ignored. The physical cross section of the blade is shown in figure 20. The physical cross section is modelled as a composite of a portion of an ellipse and a wedge joined together as shown.

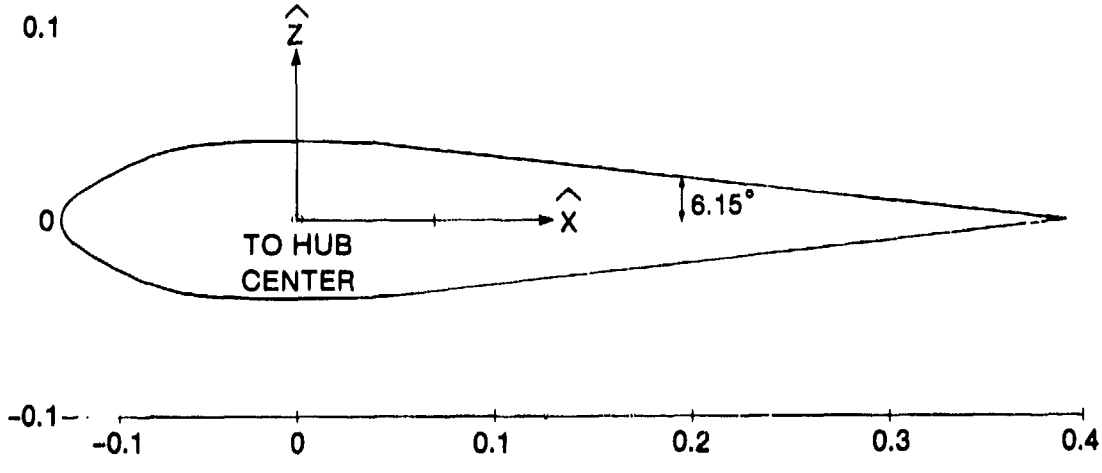

Figure 20. Hind-D rotor blade physical cross section.

Blade rotation is fully modelled by keeping track of the instantaneous value of the rotation angle θ. A constant rotation velocity of 4 rps, typical of Hind-D cruising speeds, is assumed. An arbitrary initial angle for the blade can be specified so that the fuze can be made to encounter a blade at any angle desired.

There are provisions in the model for addition of a tilt angle for the rotor assembly (so that the z-axis would not be parallel to z") and for an attack angle on each blade. However, these angles have not yet been implemented. The top and the bottom of the blade also are assumed to be identical. All of these conditions are true for the ESL model and probably are not a bad approximation of a functional blade assembly. Finally, blade droop is not addressed in the model so that the blade is assumed to be straight along the y-axis.

The rotor blade model is discussed in detail elsewhere* and the computer code also is listed.

*J. F. Dammann, Radar Backscatter Model for Hind-D Rotor Blades, Harry Diamond Laboratories.

DISTRIBUTION

ADMINISTRATOR
DEFENSE TECHNICAL INFORMATION CENTER
ATTN DTIC-DDA (12 COPIES)
CAMERON STATION, BUILDING 5
ALEXANDRIA, VA 22314

COMMANDER
US ARMY ARMAMENT MATERIEL
READINESS COMMAND
ATTN DRSAR-LEP-L, TECHNICAL LIBRARY
ATTN DRSAR-ASF, FUZE & MUNITIONS
SUPPORT DIV
ROCK ISLAND, IL 61299

COMMANDER
US ARMY MISSILE & MUNITIONS
CENTER & SCHOOL
ATTN ATSK-CTD-F
REDSTONE ARSENAL, AL 35809

DIRECTOR
US ARMY MATERIEL SYSTEMS ANALYSIS
ACTIVITY
ATTN DRXSY-MP
ABERDEEN PROVING GROUND, MD 21005

DIRECTOR
US ARMY BALLISTIC RESEARCH LABORATORY
ATTN DRDAR-TSB-S (STINFO)
ABERDEEN PROVING GROUND, MD 21005

US ARMY ELECTRONICS TECHNOLOGY
& DEVICES LABORATORY
ATTN DELET-DD
FT MONMOUTH, NJ 07703

HQ USAF/SAMI
WASHINGTON, DC 20330

COMMANDER
ATTN AD/DLYD, MR. RANDALL JONES (2 COPIES)
EGLIN AFB, FL 32542

COMMANDER
ATTN ASD-YYM, MR. PHILIP WETZEL (3 COPIES)
WRIGHT-PATTERSON AFB, OH 45433

COMMANDER
PACIFIC MISSILE TEST CENTER
ATTN CODE 1245, MR. BRUCE NOFREY
(2 COPIES)
PT MUGU, CA 93042

US ARMY ELECTRONICS RESEARCH
& DEVELOPMENT COMMAND
ATTN TECHNICAL DIRECTOR, DRDEL-CT

HARRY DIAMOND LABORATORIES
ATTN CO/TD/TSO/DIVISION DIRECTORS
ATTN RECORD COPY, 81200
ATTN HDL LIBRARY, 81100 (2 COPIES)
ATTN HDL LIBRARY, 81100 (WOODBRIDGE)
ATTN TECHNICAL REPORTS BRANCH, 81300
ATTN LEGAL OFFICE, 97000
ATTN CHAIRMAN, EDITORIAL COMMITTEE
ATTN MORRISON, R. E., 13500 (GIDEP)
ATTN CHIEF, 10000
ATTN CHIEF, 11000
ATTN CHIEF, 11100 (2 COPIES)
ATTN CHIEF, 11200
ATTN CHIEF, 11400
ATTN CHIEF, 34000
ATTN CHIEF, 34400
ATTN CHIEF, 34300
ATTN CHIEF, 15000
ATTN CHIEF, 13300
ATTN CHIEF, 36000
ATTN CHIEF, 36100
ATTN COSTANZA, J., 11400
ATTN ALEXANDER, P., 11400
ATTN LOWE, J., 11400
ATTN ARSEM, C., 11100
ATTN RODKEY, D., 36100
ATTN MINOR, M., 36100
ATTN MICHALOWICZ, J., 22100
ATTN EDWARD, C. E. H., 15400
ATTN KITCHMAN, L. A., 47500
ATTN ANTONY, R. T., 15300
ATTN DAMMANN, J. F., 11400 (20 COPIES)